

# Phonon dispersion relations, phase transitions, and thermodynamic properties of $\text{ZrSiO}_4$ : Inelastic neutron scattering experiments, shell model, and first-principles calculations

S. L. Chaplot

*Solid State Physics Division, Bhabha Atomic Research Centre, Trombay, Mumbai 400 085, India*

L. Pintschovius

*Forschungszentrum Karlsruhe, Institut für Festkörperphysik, P.O.B. 3640, D-76021 Karlsruhe, Germany  
and Laboratoire Léon Brillouin, CEA-Saclay, F-91191 Gif sur Yvette Cedex, France*

N. Choudhury and R. Mittal

*Solid State Physics Division, Bhabha Atomic Research Centre, Trombay, Mumbai 400 085, India*

(Received 19 December 2005; revised manuscript received 24 February 2006; published 31 March 2006)

Zircon,  $\text{ZrSiO}_4$ , is a geophysically important mineral for which a knowledge of the phonon spectra and interatomic potentials would be very useful for modeling the thermodynamic properties at high temperatures and high pressures. We have carried out extensive inelastic neutron scattering experiments on zircon which extend previous phonon measurements to several branches not yet studied, in particular at high energy transfer up to 85 meV. First principles density functional perturbation theory calculations of the phonon dispersion relations have been completed and found to be in agreement with the measurements. The experimental data of the phonon frequencies and the crystal structure have been used to refine an interatomic potential with a lattice dynamical shell model. The shell model calculations produce a very good description of the available data on the phonon density of states measured on a polycrystalline sample. The model is used further to calculate the structure, dynamics, and the Gibb's free energy as a function of pressure, in the zircon and scheelite phases. The free energy calculation reproduces the stability of the scheelite phases above 10 GPa as compared to the zircon phase.

DOI: [10.1103/PhysRevB.73.094308](https://doi.org/10.1103/PhysRevB.73.094308)

PACS number(s): 63.20.Dj, 78.70.Nx, 71.15.Mb

## I. INTRODUCTION

Zircon  $\text{ZrSiO}_4$  is a geophysically important material. In particular, it is an important host silicate mineral for heat producing radioactive elements uranium and thorium in the Earth's crust. The mineral is found in igneous rocks and sediments. A phase transition from the zircon to scheelite structure has been observed in static high pressure<sup>1-4</sup> and shock experiments.<sup>5</sup> The compressibility<sup>6</sup> and thermal expansion<sup>7</sup> of zircon are lowest among the oxygen based compounds. Zircon finds useful industrial applications due to its low thermal conductivity and high melting point. It is a good refractory material with a low thermal expansion and good thermal shock resistance. We note that  $\text{ZrSiO}_4$  scheelite is even more incompressible than zircon itself and is one of the most incompressible compounds<sup>8</sup> containing  $\text{SiO}_4$  tetrahedra. A high temperature neutron powder diffraction study<sup>9</sup> of zircon carried out up to 1900 K showed a displacive phase transition at 1100 K, and further decomposition into  $\text{ZrO}_2$  and  $\text{SiO}_2$  at 1750 K. Due to the various applications of zircon, several groups<sup>10-14</sup> have reported experimental and theoretical studies of its structural and vibrational properties, including the specific heat and elastic constants.<sup>15,16</sup>

For a better understanding of the  $\text{ZrSiO}_4$  phase diagram and the thermodynamic properties at high pressures and high temperatures, a knowledge of the interatomic potentials would be very useful. Accurate interatomic potentials will permit multiscale modelling of zircon which can be used to derive the phase diagram, elastic, vibrational and thermody-

amic properties at high pressures and temperatures. In the present study, we made an attempt to develop such an interatomic potential. In order to be able to refine the interatomic potential previously reported by us<sup>14</sup> we have carried out extensive phonon studies on zircon which extend previous measurements to several branches not yet studied, in particular at high energy transfer up to 85 meV. Further, density functional linear response studies<sup>17-19</sup> have been undertaken to derive the phonon dispersion relations of zircon along various high symmetry directions. The *ab initio* results are in good agreement with the inelastic neutron data and reproduce the experimental structure and phonon frequencies at least as well as the empirical shell model potential without the need of fitting to experimental data. On the other hand, an empirical potential has its merits for exploring the phase diagram and thermodynamic behavior of the material under study. As we will show, our empirical potential successfully reproduces the phase transition from the zircon to the scheelite structure under pressure.

## II. EXPERIMENT

The neutron measurements were performed in three rounds using different techniques. Our early measurements of the phonon dispersion relation in zircon were performed on the medium resolution triple axis spectrometer at Trombay.<sup>13</sup> Due to the relatively low neutron flux of this instrument, these measurements were restricted to an energy range up to 32 meV. Subsequently, further measurements<sup>14</sup>

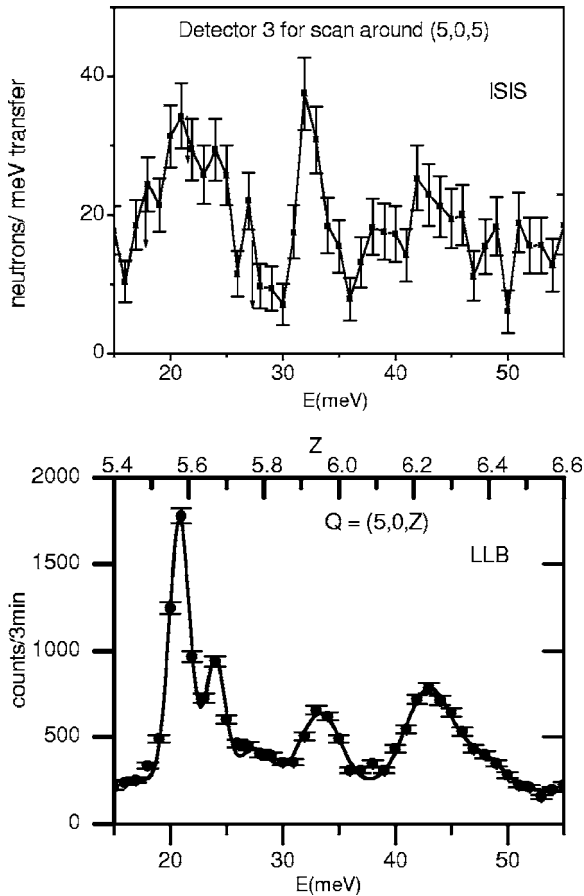


FIG. 1. The upper and lower panels correspond to neutron inelastic scattering scans performed using the PRISMA spectrometer at ISIS and 1 T spectrometer at LLB, respectively. The spectrum at LLB was collected in three hours. At ISIS eleven spectra were recorded simultaneously in 20 hours time.

were done on the PRISMA spectrometer at ISIS using time of flight technique.<sup>20</sup> The maximum phonon energies recorded on this instrument were 65 meV. These measurements yielded a large number of phonon frequencies because TOF techniques allow a simultaneous measurement of several phonons along specific paths in  $Q$ - $E$  space [we could use 11 analyzer-detector systems on the PRISMA spectrometer at ISIS (Ref. 20)]. We performed additional measurements using the 1 T triple axis spectrometer at the Laboratoire Léon Brillouin, Saclay. This instrument is equipped with vertically and horizontally focusing monochromators and analyzers resulting in a high neutron intensity. Measurements in the (100)-(010) scattering plane were done with Cu111 and pyrolythic graphite (PG002) as a monochromator and analyzer, respectively. This configuration gave a higher intensity than that of the PRISMA spectrometer, but a lower resolution. Further measurements in the (100)-(001) scattering plane were done with Cu220 as a monochromator. This reduced the intensity by nearly a factor of 3 but improved the resolution considerably. Figure 1 shows a comparison of two scans taken along a similar path in  $(Q, E)$  space on the PRISMA spectrometer and the 1 T spectrometer with Cu220 as monochromator. The superiority of the triple axis spectrometer

with this particular setup is obvious for such type of measurements.

All the phonon dispersion measurements discussed here were carried out on the same natural single crystal of about 4 cm<sup>3</sup> obtained from the mining site at Puttetti, Tamilnadu, India. It contains 0.9% of hafnium by weight as the main impurity. The crystal was cooled to 10 K in a helium cryostat.

### III. LATTICE DYNAMICAL CALCULATIONS

Lattice dynamical calculations are essential for the planning of neutron experiments, i.e., for the calculation of the one-phonon structure factors in order to select the most appropriate Bragg points for the detection of particular phonons. Furthermore, they are very important for assignments of the various inelastic signals to specific phonon branches.

Lattice dynamical calculations require information about the interatomic forces that can be obtained either by using a quantum-mechanical *ab initio* formulation or by using semi-empirical interatomic potentials. Density functional theory calculations of the zone-center phonons using the local density approximation (LDA), have been reported.<sup>12</sup> We have studied the phonon dispersion relations along the various high symmetry directions in the Brillouin zone using the same extended norm conserving pseudopotentials used earlier.<sup>12</sup> These calculations within the LDA have been carried out using plane wave basis sets and the code ABINIT,<sup>21</sup> using the supercomputing resources at the Bhabha Atomic Research Centre. The Brillouin zone integrations were performed with a  $4 \times 4 \times 4$   $\mathbf{k}$ -point mesh using a plane wave energy cutoff of 70 Ry. In addition, we have refined the earlier interatomic potentials<sup>14</sup> using the crystal structure of zircon and the present phonon data at the zone center and zone boundary. Hereby, we were aiming at a potential that is transferable to other structures.

The interatomic potential used here consists of Coulombic and short-ranged Born-Mayer type interaction terms

$$V(r) = \left\{ \frac{e^2}{4\pi\epsilon_0} \right\} \left\{ \frac{Z(k)Z(k')}{r} \right\} + a \exp \left\{ \frac{-br}{R(k) + R(k')} \right\} - \frac{C}{r^6}. \tag{1}$$

Here  $r$  is the separation between the atoms of a type  $k$  and  $k'$ .  $R(k)$  and  $Z(k)$  are the effective radius and charge of the  $k$ th atom type. We have treated  $a=1822$  eV and  $b=12.364$  as constants; this choice has been successfully used earlier in the lattice dynamical calculations of several complex solids.<sup>22,23</sup> The van der Waals interaction in Eq. (1) (last term) is applied only between the oxygen atoms. We have also included a Si-O bond stretching potential of the form

$$V(r) = -D \exp[-n(r - r_o)^2/(2r)]. \tag{2}$$

The parameters used in our calculations are  $Z(\text{Zr})=3.50$ ,  $Z(\text{Si})=2.54$ ,  $Z(\text{O})=-1.51$ ,  $R(\text{Zr})=1.93$  Å,  $R(\text{Si})=0.83$  Å,

TABLE I. Comparison between the experiment<sup>a,b</sup> (at 293 K) and calculated structural parameters (at 0 K) of zircon and scheelite phase of ZrSiO<sub>4</sub>. For zircon structure (body centered tetragonal,  $I4_1/amd$ ) the Zr, Si, and O atoms are located at (0, 0.75, 0.125), (0, 0.25, 0.375), and (0,  $u, v$ ), respectively, and their symmetry equivalent positions. For scheelite structure (body centered tetragonal,  $I4_1/a$ ) the Zr, Si, and O atoms are located at (0, 0, 0.5), (0, 0, 0), and ( $u, v, w$ ), respectively, and their symmetry equivalent positions.

	Experiment <sup>b</sup> (Zircon)	Calculated shell model (Zircon)	Calculated <sup>c</sup> <i>ab-initio</i> (Zircon)	Experiment <sup>a</sup> (Scheelite)	Calculated (Scheelite)
$a$ (Å)	6.610	6.51	6.54	4.726	4.70
$c$ (Å)	6.001	6.08	5.92	10.515	10.71
$u$	0.0646	0.071	0.0645		0.252
$v$	0.1967	0.208	0.1945		0.143
$w$					0.070

<sup>a</sup>Reference 4(a).

<sup>b</sup>Reference 24.

<sup>c</sup>Reference 12.

$R(O)=1.9$  Å,  $C=100$  eV Å<sup>6</sup>,  $D=1.1$  eV,  $n=24.0$  Å<sup>-1</sup>,  $r_o=1.627$  Å. The polarizability of the oxygen atoms is introduced in the framework of the shell model<sup>25,26</sup> with the shell charge  $Y(O)=-2.68$  and shell-core force constant  $K(O)=110$  eV Å<sup>-2</sup>. The crystal structure at any pressure (at zero temperature) is obtained by minimization of the enthalpy. At ambient pressure the calculated structure (Table I) is in good agreement with the available experimental data.<sup>24</sup> The lattice dynamics calculations are carried out in the quasiharmonic approximation. The shell model calculations have been carried out using the current version of the code DISPR (Ref. 27) developed at Trombay.

### IV. RESULTS

#### A. Crystal structure, group theoretical analysis, and long wavelength lattice dynamics

Zircon, ZrSiO<sub>4</sub> has a body centered tetragonal structure (Fig. 2) with space group  $I4_1/amd$  and two formula units per primitive cell. Neutron diffraction studies on a single crystal<sup>21</sup> and polycrystalline samples<sup>9</sup> are available. The Zr and Si atoms occur at special positions  $4a$  and  $4b$ , respectively, whereas O atoms occur at  $16h$ . The principle structure unit can be considered as a chain of alternating edge-sharing SiO<sub>4</sub> tetrahedra and ZrO<sub>8</sub> triangular dodecahedra extending

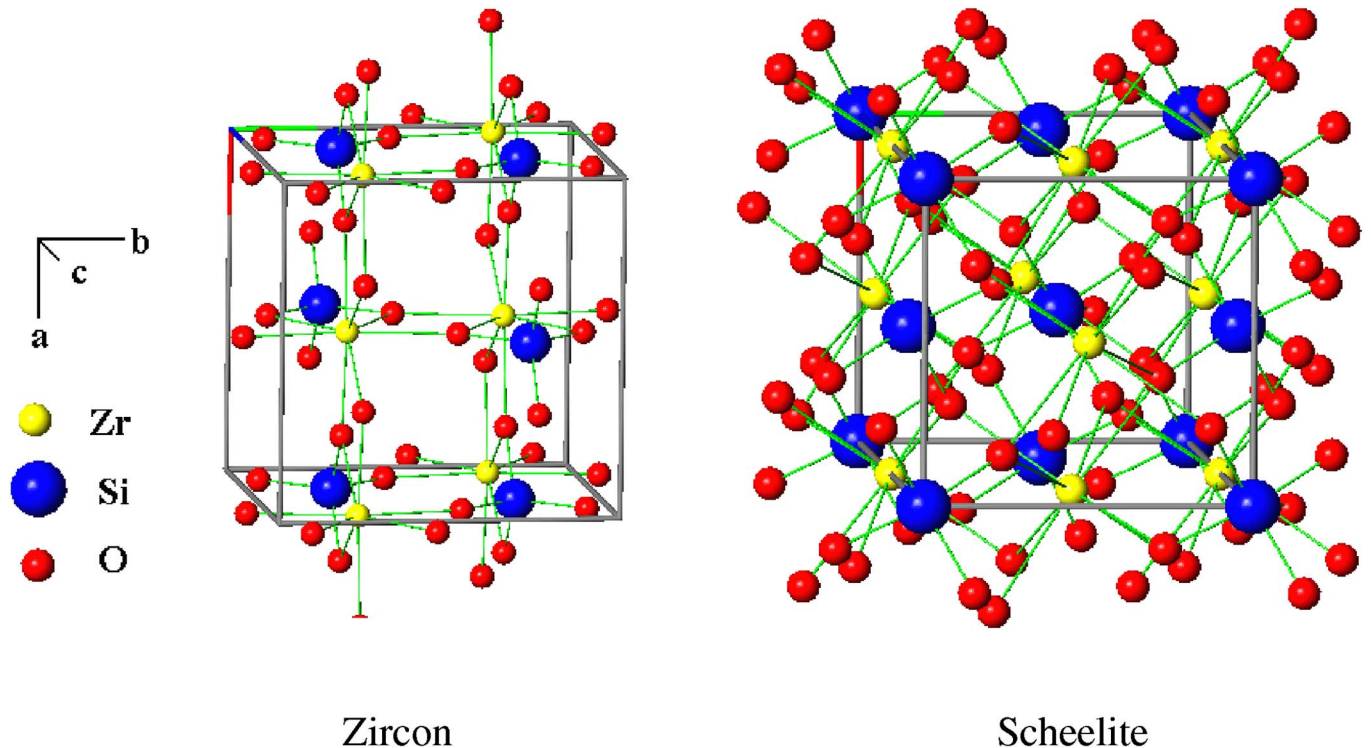


FIG. 2. (Color online) Ball and stick representation of the zircon (space group  $I4_1/amd$ ) and scheelite ( $I4_1/a$ ) phases of ZrSiO<sub>4</sub>.

parallel to the *c*-axis, with the chain joined along the *a*-axis by edge-sharing ZrO<sub>8</sub> dodecahedra. As can be inferred from Table I, the computed structure obtained both from shell model potentials and first principles are in good agreement with experiment.

Group theoretical symmetry analysis was undertaken to classify the phonon modes belonging to various representations. This enables direct comparisons with observed single crystal Raman, infrared and inelastic neutron data. Because of the selection rules only phonon modes belonging to certain group theoretical representations are active in typical single crystal Raman, infrared and inelastic neutron scattering measurements. These selection rules are governed by the symmetry of the system and the scattering geometry employed. The theoretical scheme for the derivation of the symmetry vectors is based on irreducible multiplier representations and described in detail in Ref. 25 This involves construction of symmetry adapted vectors,<sup>28</sup> which are used for block diagonalizing the dynamical matrix and then, for the assignment of the phonon modes belonging to various representations.

The phonon branches at the  $\Gamma$  point, and along the  $\Delta$ ,  $\Lambda$ , and  $\Sigma$  directions decompose as follows:

$$\Gamma: 2A_{1g} + A_{2g} + A_{1u} + 4A_{2u} + 4B_{1g} + B_{2g} + B_{1u} + 2B_{2u} + 5E_g + 5E_u,$$

$$\Delta: 11\Delta_1 + 7\Delta_2 + 11\Delta_3 + 7\Delta_4,$$

$$\Lambda: 6\Lambda_1 + 2\Lambda_2 + 6\Lambda_3 + 2\Lambda_4 + 10\Lambda_5,$$

$$\Sigma: 8\Sigma_1 + 8\Sigma_2 + 10\Sigma_3 + 10\Sigma_4.$$

The zone center,  $A_{1g}$ ,  $B_{1g}$ ,  $B_{2g}$ , and  $E_g$  modes are Raman active, and  $E_u$  and  $A_{2u}$  modes are infrared active. The  $E_g$  and  $E_u$  modes are doubly degenerate. The  $A_{1u}$ ,  $A_{2g}$ ,  $B_{1u}$ , and  $B_{2u}$  modes are optically inactive, but can be observed using inelastic neutron scattering. The  $A_{2u}$  and  $E_u$  modes are polar modes exhibiting LO-TO splittings, with their macroscopic field, respectively, parallel and perpendicular to the tetragonal *c* axis. The computed long wavelength phonon modes (Table II) are found to be in good agreement with the present inelastic neutron experiments and reported Raman and infrared data.<sup>12</sup> The shell model long wavelength results show a satisfactory agreement with the experimental data<sup>12</sup> with an average deviation of 4% as seen in Table II. *Ab initio* calculations agree better with experiments with a 2% average deviation (Table II).

### B. Phonon dispersion relations

The symmetry assignments and phonon dispersion relations results from the present inelastic neutron scattering experiments are shown in Fig. 3 along with those from earlier

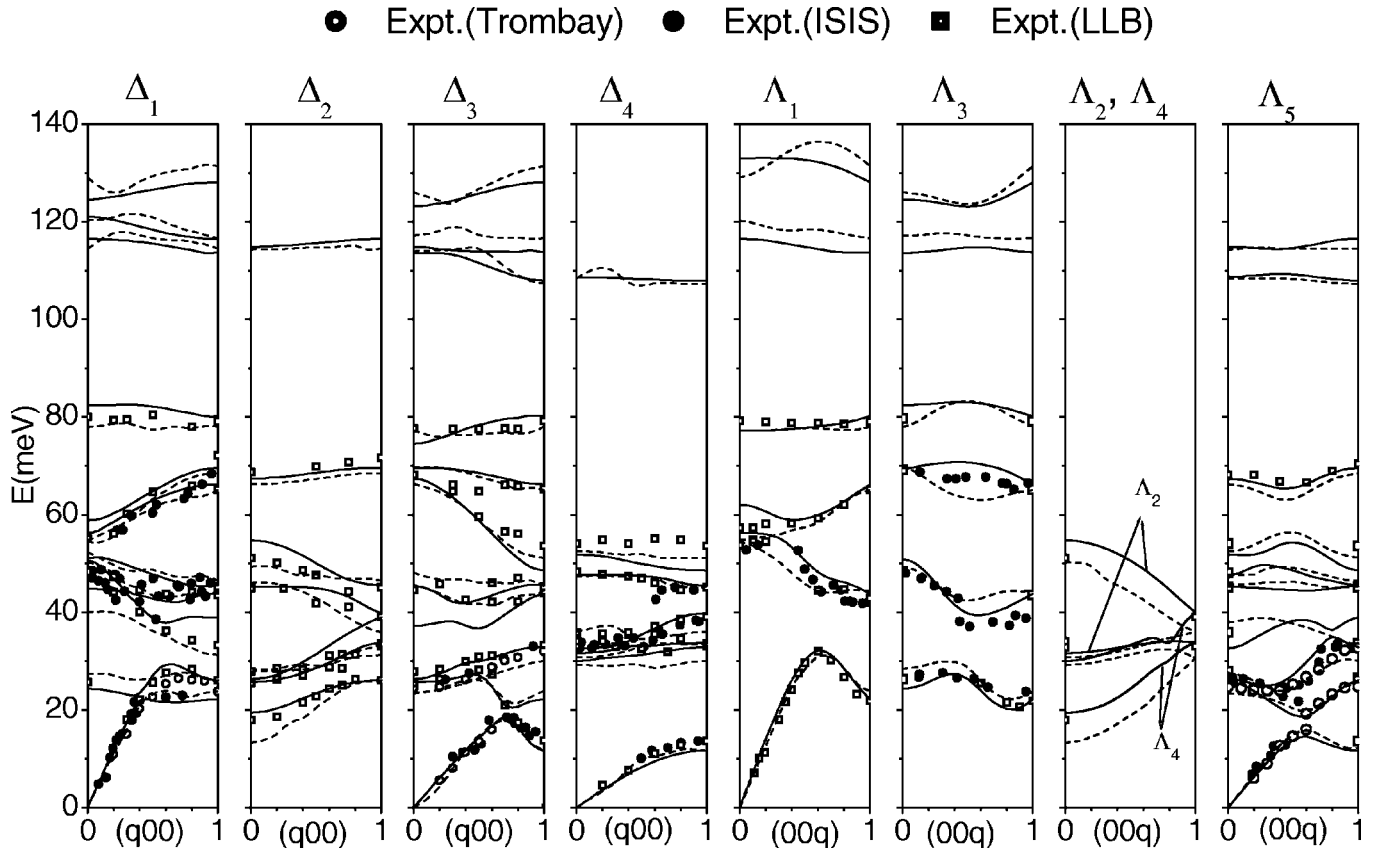


FIG. 3. The experimental phonon dispersion curves in zirconon along with the lattice dynamical calculations (solid lines for shell model, dashed lines for *ab initio*) for zirconon. The open rectangles, solid circles and open circles give the phonon peaks identified in the experiments at LLB (France), ISIS (Ref. 14) (UK), and Dhruva (Ref. 13) (India), respectively.

TABLE II. Comparison of the experimental and calculated zone centre optic phonon modes in meV units. The present first principles density functional studies use the same code and pseudopotentials as Rignanese *et al.*<sup>a</sup> and the long wavelength results are identical. The results obtained using the fitted shell model are also given.

	Raman and IR modes Ref. 10(a)	Ref. 10(b)	Present neutron experiment	Calculated <i>Ab initio</i> (Ref. 12)	Calculated (shell model)
$A_{1g}$	54.5		53.5	54.8	56.2
	120.9			120.5	116.5
$A_{2g}$			32.7	30.0	31.7
$B_{1g}$	26.6		26.2	27.9	24.4
	48.8		48.2	49.3	50.8
			82.0	78.4	82.4
	125.1			126.2	124.6
$B_{2g}$	33.0		34.0	31.3	30.0
$E_g$	24.9		25.4	24.1	25.8
	27.9		27.8	27.9	26.3
	44.3		44.8	46.5	45.3
			68.6	66.5	67.4
	125.1			114.5	114.9
$A_{1u}$			51.0	48.7	54.7
$B_{1u}$			17.8	14.8	19.4
$B_{2u}$				70.3	69.5
				117.1	113.6
$A_{2u}(\text{LO})$	59.6	59.3	56.2	59.1	62.0
	75.4	79.7	76.6	80.2	77.2
	137.5	136.5		136.0	133.0
$A_{2u}(\text{TO})$		42.1		43.2	37.2
		75.2	79.5	74.6	74.5
		121.2		121.6	123.2
$E_u(\text{LO})$		43.9		42.3	44.8
		51.7		52.1	51.8
		58.1		57.8	58.8
		128.3		127.7	121.0
$E_u(\text{TO})$	35.6	34.9	35.8	35.4	32.6
	48.4	47.3	48.2	47.5	47.6
	53.5	53.2	54.0	52.4	51.8
	109.8	108.1		107.6	108.7

<sup>a</sup>Reference 12.

experiments at Dhruva (India) and ISIS (UK). Due to the involved nature of these experiments, such extensive measurements are often not available despite their importance. The measured data are compared with the computed first principles results and the fitted results obtained using the shell model. The present experimental results are generally in very good agreement with the earlier ones<sup>13,14</sup> wherever available and also in agreement with the first principles calculations. The quality of the fit is also satisfactory with about 4% deviation between the experimental and the calculated shell model values. The observed phonon intensities are found to be in good qualitative agreement with the calculated one-phonon structure factors, which is quite satisfactory considering the many corrections involved in the experimental

intensities and the difficulties generally encountered when making predictions from models.

### C. Elastic constants, thermodynamic properties, and high pressure phase transitions

As stated above, an important objective of the present work was to develop accurate interatomic potentials for zircon in order to derive various macroscopic properties over a wide range of pressure and temperature. Thus the interatomic potentials developed in this study have been used to compute various properties. The calculated phonon density of states obtained by integrating over the phonon modes in the whole Brillouin zone and its comparison with available neutron

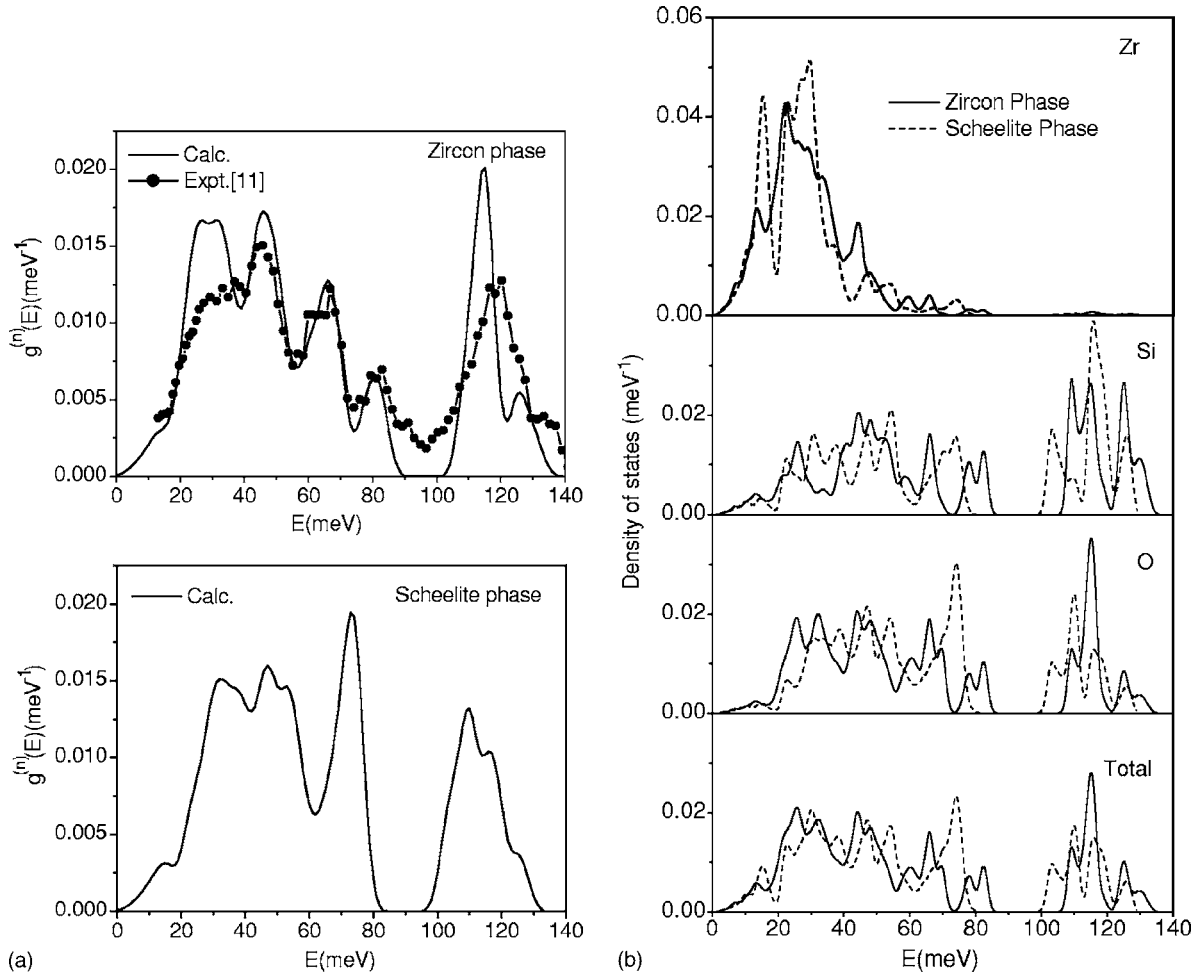


FIG. 4. (a) The comparison of the measured (Ref. 11) (solid circles) and calculated (solid line, shell model) neutron-cross-section-weighted phonon density of states in zircon. The line through the solid circles is only a guide to the eye. The calculated phonon density of states for scheelite phase is also shown in lower panel. The multiphonon contribution has been subtracted from experimental data to obtain the experimental one-phonon spectrum. (b) The calculated partial density of states of various atoms and total density of states of  $\text{ZrSiO}_4$  in zircon and scheelite phase.

scattering data from polycrystalline sample<sup>11</sup> is shown in Fig. 4(a). The agreement between the two is quite satisfactory in terms of the various peak positions although the peak at 25  $\text{meV}$  appears stronger in the calculations. Both the experimental inelastic neutron powder data and calculation show a band gap in the frequency range from 90 to 110  $\text{meV}$ . This band gap is also obtained from the present single crystal inelastic neutron data. For the Si-O stretching modes around 120  $\text{meV}$ , the experiment shows a single broad peak while the calculations indicate separated peaks. However, the experimental resolution might have been insufficient to resolve the small peak at 128  $\text{meV}$  predicted by our calculations. We have also given predictions of the phonon density of states in the scheelite phase from the present potential. Figure 4(b) provides the partial contributions to the density of states from various atomic species. We further note that the computed elastic constants (Table III), equation of state (Fig. 5), and specific heat (Fig. 6) obtained from the shell model, are also in good agreement with reported experiments. The reported experimental values of the bulk modulus in the scheelite phase are 392 [ Ref. 4(c) ] and

301 GPa (Ref. 8) which are very different from each other, the latter is close to the calculated value of 303 GPa. The

TABLE III. Comparison between the experimental<sup>a</sup> and calculated elastic constants and bulk modulus of  $\text{ZrSiO}_4$  in zircon and scheelite phases (in GPa units). The experimental data of bulk modulus (B) is from Refs. 4(c) and 8. Calculated bulk modulus is from calculated elastic constants.

Elastic constant	Experiment (Zircon)	Calculated (Zircon)	Experiment (Scheelite)	Calculated (Scheelite)
$C_{11}$	424.4	432		470
$C_{33}$	489.6	532		288
$C_{44}$	113.3	110		74
$C_{66}$	48.2	39		133
$C_{12}$	69.2	73		241
$C_{13}$	150.2	180		255
$B$	205(8)	251	392(9), 301(12)	303

<sup>a</sup>Reference 16.

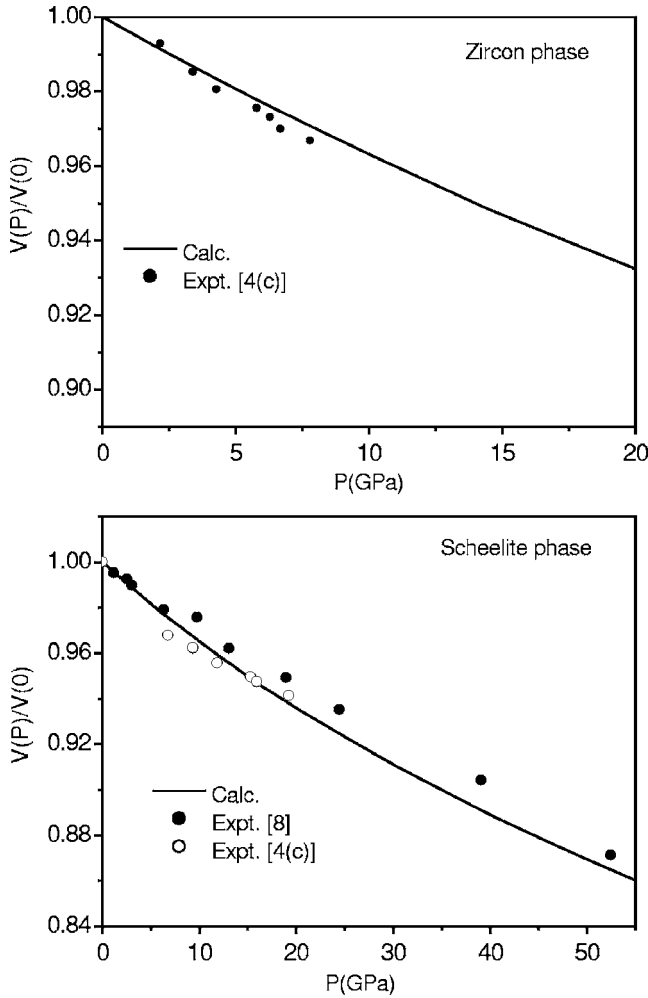


FIG. 5. The comparison between the calculated and experimental (Ref. 4) equation of state of  $ZrSiO_4$  in zircon and scheelite phases.

former value is difficult to understand since the measured equation of state appears in good agreement with calculations. The difference probably arises from fitting procedure

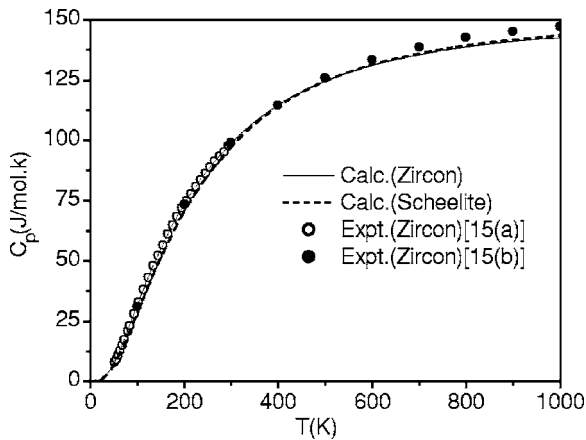


FIG. 6. The comparison between the calculated and experimental (Ref. 15) specific heat of  $ZrSiO_4$  in zircon phase. The calculated  $C_p$  in scheelite phase is shown by the dashed line.

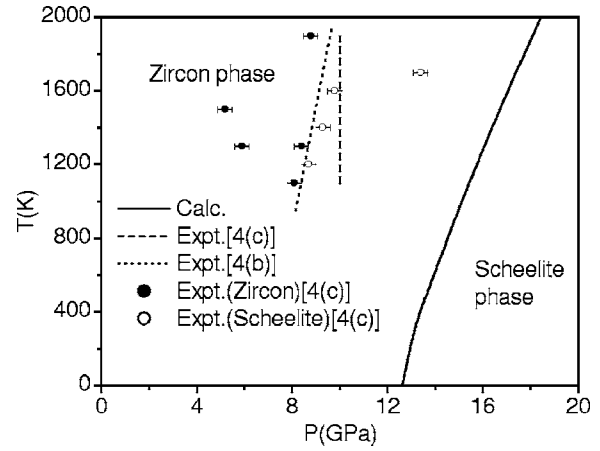


FIG. 7. The calculated phase diagram of zircon as obtained from the free energy calculations in the zircon and scheelite phases of  $ZrSiO_4$ . The experimental observations (Ref. 4) of stable phases and phase boundary are also shown.

used in deriving the experimental values of the bulk modulus.

A phase transition from zircon to scheelite structure has been observed in  $ZrSiO_4$  at high pressures. The interatomic potential developed for the zircon phase has been used for the lattice dynamical calculations in the scheelite phase. The stability of a crystalline phase is determined by the minimization of the Gibbs free energy. The calculated structure (Fig. 2) of the scheelite phase is given in Table I. We have calculated Gibbs free energies including the complete vibrational contributions as a function of pressure up to 20 GPa and temperature up to 2000 K in the zircon as well as the high-pressure scheelite phase. The free energy calculation reproduces the stability of the scheelite phases above about 10 GPa (Fig. 7) as compared to the zircon phase, in good agreement with experiments. This is highly satisfactory since usually it is very difficult to reproduce free energy differences with requisite high accuracy for phase diagram calculation. It is also a very difficult task to identify equilibrium phases from experiments at high pressure due to large hysteresis often found at low temperature.

### V. CONCLUSIONS

This paper reports a significant extension of our previous lattice dynamical studies of the mineral zircon using the technique of neutron inelastic scattering in combination with first principles studies and a lattice dynamical shell model. Nearly complete experimental data are now available on the phonon dispersion relation in two high-symmetry directions up to 85 meV. The *ab initio* calculations reproduce the experimental data on the structure and the vibrational properties very well. The agreement between calculation and experiment is slightly worse for the shell model but is still quite satisfactory. Further quantities derived from the model, i.e., the elastic constants, equation of state, density of states, and specific heat computed using the fitted potentials are all found to be in good agreement with experiments. Moreover the model has the advantage that it can easily be used for

calculating the free energies as a function of pressure up to 20 GPa and temperature up to 2000 K in the zircon as well as the high-pressure scheelite phase. Thus, it is possible to explore the relative stability of the two phases, zircon and scheelite, across their observed phase transition pressure of about 10 GPa. We found that observed phase diagram is very satisfactorily reproduced by our calculations. This means that the potential derived in the present work can be fruitfully used to understand the high pressure and temperature phase diagram, thermodynamic properties and various microscopic

and macroscopic properties of zircon using a combination of techniques like lattice dynamics calculations and molecular dynamics simulations.

### ACKNOWLEDGMENTS

We thank Computer Division, BARC for providing super-computing facilities and in particular, K. Rajesh for technical support with parallel computing.

- 
- <sup>1</sup>A. F. Reid and A. E. Ringwood, *Earth Planet. Sci. Lett.* **6**, 205 (1969).
- <sup>2</sup>A. E. Ringwood, *Composition and Petrology of the Earth's Mantle* (McGraw-Hill, New York, 1975).
- <sup>3</sup>L. G. Liu, *Earth Planet. Sci. Lett.* **44**, 390 (1979).
- <sup>4</sup>(a) E. Knittle and Q. Williams, *Am. Mineral.* **78**, 245 (1993); (b) S. Ono, K. Funakoshi, Y. Nakajima, Y. Tange, and T. Katsura, *Contrib. Mineral. Petrol.* **147**, 505 (2004); (c) S. Ono, Y. Tange, I. Katayama, and T. Kikegawa, *Am. Mineral.* **89**, 185 (2004).
- <sup>5</sup>K. Kusuba, Y. Syono, M. Kikuchi, and K. Fukuoka, *Earth Planet. Sci. Lett.* **72**, 433 (1985).
- <sup>6</sup>D. B. Siredeshmukh and K. G. Subhadra, *J. Appl. Phys.* **46**, 3682 (1975); R. M. Hagen and L. W. Finger, *Am. Mineral.* **64**, 196 (1979).
- <sup>7</sup>A. J. Falzone and F. D. Stacey, *Phys. Chem. Miner.* **8**, 212 (1982); T. G. Worlton, L. Cartz, A. Niravath, and H. Ozkan, *High Temp. - High Press.* **4**, 463 (1972); E. C. Subbarao, D. K. Agarwal, H. A. McKinstry, C. W. Salles, and R. Roy, *J. Am. Ceram. Soc.* **73**, 1246 (1989); J. B. Austin, *ibid.* **14**, 795 (1931); E. C. Subbarao and K. U. G. K. Gokhale, *Jpn. J. Appl. Phys.* **7**, 1126 (1968).
- <sup>8</sup>H. P. Scott, Q. Williams, and E. Knittle, *Phys. Rev. Lett.* **88**, 015506 (2001).
- <sup>9</sup>Z. Mursic, T. Vogt, and F. Fray, *Acta Crystallogr., Sect. B: Struct. Sci.* **B48**, 584 (1992).
- <sup>10</sup>(a) P. Dawson, M. M. Hargreave, and G. R. Wilkinson, *J. Phys. C* **4**, 240 (1971); (b) F. Gervais, B. Piriou, and F. Cabannes, *J. Phys. Chem. Solids* **34**, 1785 (1973).
- <sup>11</sup>J. C. Nipko and C.-K. Loong, *Physica B* **241**, 415 (1998).
- <sup>12</sup>G. M. Rignanese, X. Gonze, and A. Pasquarello, *Phys. Rev. B* **63**, 104305 (2001).
- <sup>13</sup>R. Mittal, S. L. Chaplot, Mala N. Rao, N. Choudhury, and R. Parthasarthy, *Physica B* **241**, 403 (1998).
- <sup>14</sup>R. Mittal, S. L. Chaplot, R. Parthasarathy, M. J. Bull, and M. J. Harris, *Phys. Rev. B* **62**, 12089 (2000).
- <sup>15</sup>(a) K. K. Kelly, *J. Am. Chem. Soc.* **63**, 2750 (1941); (b) D. R. Stull and H. Prophet, *JANAF Thermochemical Tables*, 2nd ed. (National Bureau of Standards, Washington, D.C, 1971).
- <sup>16</sup>H. Ozkan and J. C. Jamieson, *Phys. Chem. Miner.* **2**, 215 (1978).
- <sup>17</sup>S. Baroni, S. de Gironcoli, A. D. Corso, and P. Giannozzi, *Rev. Mod. Phys.* **73**, 515 (2001); S. Baroni, P. Giannozzi, and A. Testa, *Phys. Rev. Lett.* **58**, 1861 (1987); P. Giannozzi, S. de Gironcoli, P. Pavone, and S. Baroni, *Phys. Rev. B* **43**, 7231 (1991).
- <sup>18</sup>M. C. Payne, M. P. Teter, D. C. Allan, T. A. Arias, and J. D. Joannopoulos, *Rev. Mod. Phys.* **64**, 1045 (1992).
- <sup>19</sup>X. Gonze, D. C. Allan, and M. P. Teter, *Phys. Rev. Lett.* **68**, 3603 (1992); X. Gonze, *Phys. Rev. B* **54**, 4383 (1996); **55**, 10337 (1997); X. Gonze and C. Lee, *ibid.* **55**, 10355 (1997).
- <sup>20</sup>U. Steigenberger, M. Hagen, R. Caciuffo, C. Petrillo, F. Cilloco, and F. Sacchetti, *Nucl. Instrum. Methods Phys. Res. B* **53**, 87 (1991).
- <sup>21</sup>The ABINIT code is a collaborative project of the Universite Catholique de Louvain, Corning Inc. and other collaborators (URL: <http://www.abinit.org/>); X. Gonze, J. -M. Beuken, R. Caracas, F. Detraux, M. Fuchs, G. -M. Rignanese, L. Sindic, M. Verstraete, G. Zerah, F. Jollet, M. Torrent, A. Roy, M. Mikami, Ph. Ghosez, J.-Y. Raty, and D. C. Allan, *Comput. Mater. Sci.* **25**, 478 (2002).
- <sup>22</sup>R. Mittal and S. L. Chaplot, *Phys. Rev. B* **60**, 7234 (1999).
- <sup>23</sup>R. Mittal, S. L. Chaplot, and N. Choudhury, *Phys. Rev. B* **64**, 094302 (2001).
- <sup>24</sup>Z. Mursic, T. Vogt, H. Boysen, and F. Frey, *J. Appl. Crystallogr.* **25**, 519 (1992).
- <sup>25</sup>A. A. Maradudin and S. H. Vosko, *Rev. Mod. Phys.* **40**, 1 (1968); G. Venkataraman, L. Feldkamp, and V. C. Sahni, *Dynamics of Perfect Crystals* (MIT Press, Cambridge, 1975).
- <sup>26</sup>P. Bruesch, *Phonons: Theory and Experiments I* (Springer-Verlag, Berlin, 1982).
- <sup>27</sup>S. L. Chaplot (unpublished).
- <sup>28</sup>O. V. Kovalev, *Irreducible Representations of Space Groups* (Gordon and Breach, New York, 1964); C. J. Bradley and A. P. Cracknell, *The Mathematical Theory of Symmetry in Solids* (Oxford University Press, Oxford, 1972).